

Metapopulation models imply non-Poissonian statistics of interevent times

Elohim Fonseca dos Reis¹ and Naoki Masuda^{1,2,*}

¹*Department of Mathematics, State University of New York at Buffalo, Buffalo, New York, USA*
²*Computational and Data-Enabled Science and Engineering Program,
State University of New York at Buffalo, Buffalo, New York, USA*

(Dated: June 22, 2021)

Interevent times in temporal contact data from humans and animals typically obey heavy-tailed distributions, and this property impacts contagion and other dynamical processes on networks. We theoretically show that distributions of interevent times heavier-tailed than exponential distributions are a consequence of the most basic metapopulation model used in epidemiology and ecology, in which individuals move from a patch to another according to the simple random walk. Our results hold true irrespectively of the network structure and also for more realistic mobility rules such as high-order random walks and the recurrent mobility patterns used for modeling human dynamics.

Introduction—Contact networks among individuals crucially impact contagion in populations and networks. In addition to the network structure, temporal aspects of contacts and edges in networks, collectively referred to as temporal networks, play a central role in such dynamics [1–4]. The interevent time (IET), defined as the time between consecutive events, is one such aspect. Event-driven stochastic dynamics models on networks most typically assume Poisson processes for generating events, which yield exponential IET distributions. However, IETs from various human activity data obey non-Poissonian statistics, in particular, heavy-tailed distributions [1, 3, 5, 6]. In most (but not all) cases, heavy-tailed IET distributions slow down contagion and diffusion in epidemic processes [7–14], opinion dynamics [15–18], evolutionary game dynamics [19], cascade processes [20–23], and random walks [24–27]. Several mechanisms can generate heavy-tailed IET distributions, including priority queue models [5, 6, 28–32], self-exciting processes [33–35], mixture of exponentials [36–38], and dynamics of nodal states, where mutual agreement of two nodes produces contact events at a high rate [39].

However, these models do not explain the genesis of heavy-tailed IET distributions present in one dominant case of human (and animal) activity—mobility. In fact, most of face-to-face contact or proximity data have been collected from mobile individuals, and such data show heavy-tailed IET distributions [25, 39–47]. Mobility constrains the statistics of IETs because contact events may occur only when individuals are copresent in the same place. For example, random walkers with heterogeneous attractiveness values moving in a plane can generate heavy-tailed IET distributions [48–51].

A prevalent approach to simultaneous modeling of mobility and agent-to-agent interaction is metapopulation models [52], originally introduced in mathematical epidemiology [53–57] and ecology [58–60]. In a metapopulation network, nodes represent subpopulations, such as, households, cities, urban areas, or ecological habitats,

and edges represent migration routes. Metapopulation models have been successful in describing, e.g., epidemic processes [2, 13, 61–63] including the COVID-19 pandemic [64].

In the present study, we provide accounts of heavy-tailed IET distributions when individuals move around, meet, and separate according to a standard metapopulation network model and its more realistic variants. We analytically show that the IET distribution for a pair of individuals is a mixture of exponential distributions, which robustly holds true for different network structures and mobility rules. Crucially, mixtures of exponential distributions produce IET distributions that are substantially closer to heavy-tailed distributions observed in empirical data than exponential distributions do.

Model—We consider a metapopulation network with N subpopulations (i.e., nodes). The network may be directed and/or weighted. The individuals that populate the network are assumed to be simple random walkers in continuous time. Different walkers move independently of each other and may produce contact events (events for short) between them when they are copresent in the same subpopulation.

Each walker diffuses from one subpopulation to an adjacent subpopulation at rate \mathcal{D} . The mobility and contact dynamics are illustrated in Fig. 1. When the walker leaves the i th subpopulation, it moves to a neighboring j th subpopulation with probability $A_{ij} / \sum_{\ell=1}^N A_{i\ell}$, where A_{ij} is the weight of edge (i, j) . Events between a pair of walkers in the same subpopulation occur according to a Poisson process with rate λ , which epidemic process models on metapopulation networks usually assume. In other words, the distribution of time t to the next event between a pair of walkers in the same subpopulation is given by $\phi_e(t) = \lambda e^{-\lambda t}$. When the walkers are in different subpopulations, no event occurs between them.

Analysis—We derive the probability density of an IET, τ , between an arbitrary pair of individuals, which are random walkers. When the two walkers are copresent in a subpopulation, events (including the case of 0 event) occur between them before either walker leaves the subpopulation. After that, a series of n copresences occurs

* naokimas@buffalo.edu

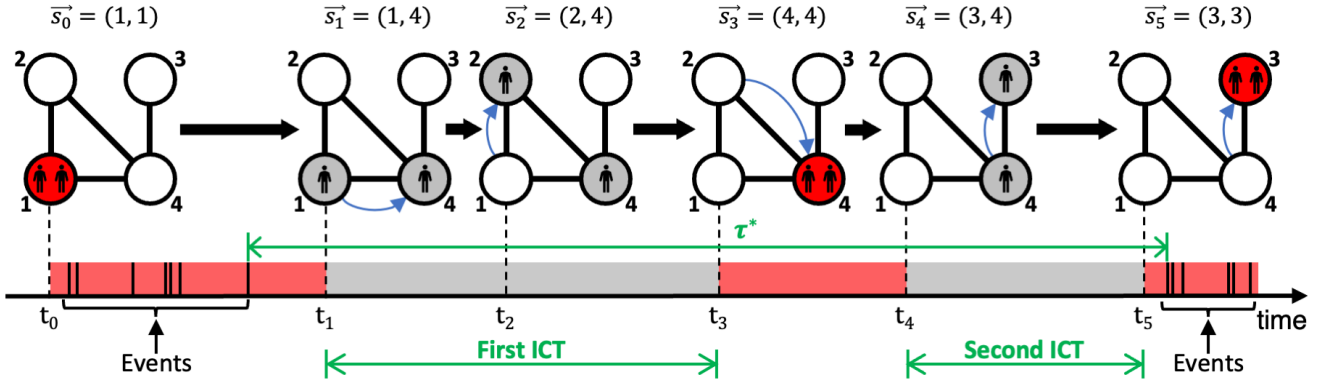


FIG. 1. Schematic illustration of the dynamics of two walkers. Initially, at $t = t_0$, the walkers are copresent in subpopulation 1. Then, events between them occur before t_1 . At $t = t_1$, one walker moves from subpopulation 1 to subpopulation 4. At $t = t_2$, the other walker moves from subpopulation 1 to subpopulation 2. At $t = t_3$, the same walker moves to subpopulation 4 to be copresent with the other walker. Therefore, the first ICT is given by $t_3 - t_1$. Although the walkers are copresent for $t \in (t_3, t_4)$, no event occurs. At $t = t_4$, one walker moves to subpopulation 3. At $t = t_5$, the other walker also moves to subpopulation 3, producing a second ICT, which is equal to $t_5 - t_4$. Finally, an event occurs during their copresence in subpopulation 3, yielding an IET, denoted by τ^* . In this example, this IET is followed by several much shorter IETs.

before the next event occurs (see Fig.1).

We let $p(\tau, n)$ be the probability of generating an IET of length τ after n copresences, where $n \in \{0, 1, 2, \dots\}$. The probability density of the time at which either walker leaves the subpopulation where the two walkers are copresent is given by $\phi_d(t) = 2\mathcal{D}e^{-2\mathcal{D}t}$. We obtain

$$p(\tau, 0) = \int_{\tau}^{\infty} dt' \phi_d(t') \int_{\tau}^{\infty} dt'' \phi_e(t'') \lambda = \lambda e^{-(\lambda+2\mathcal{D})\tau}. \quad (1)$$

By Laplace transforming $p(\tau, 0)$, we obtain $\hat{p}(s, 0) \equiv \int_0^{\infty} d\tau e^{-s\tau} p(\tau, 0) = \lambda/(s + \lambda + 2\mathcal{D})$.

We denote the distribution of time t between consecutive copresences of the two walkers, which we refer to as the inter-copresence time (ICT), by $\phi_c(t)$. Then, the joint probability density of τ and $n = 1$ is given by

$$\begin{aligned} p(\tau, 1) &= \int_0^{\tau} dt_1 S_e(t_1) S_d(t_1) 2\mathcal{D} \int_{t_1}^{\tau} dt_2 S_c(t_2 - t_1) \\ &\quad \times h_c(t_2 - t_1) S_d(\tau - t_2) S_e(\tau - t_2) \lambda \\ &= 2\mathcal{D} \lambda \int_0^{\tau} dt_1 \int_{t_1}^{\tau} dt_2 S_d(t_1) S_e(t_1) \phi_c(t_2 - t_1) \\ &\quad \times S_d(\tau - t_2) S_e(\tau - t_2). \end{aligned} \quad (2)$$

where $S_e(t) = e^{-\lambda t}$ and $S_d(t) = e^{-2\mathcal{D}t}$ are the survival functions of $\phi_e(t)$ and $\phi_d(t)$, respectively, and $S_c(t) = \int_t^{\infty} dt' \phi_c(t')$ and $h_c(t) = \phi_c(t)/S_c(t)$ are the survival and hazard functions of $\phi_c(t)$, respectively. By Laplace transforming $p(\tau, 1)$, we obtain $\hat{p}(s, 1) = 2\lambda\mathcal{D}\hat{\phi}_c(s)/(s + \lambda + 2\mathcal{D})^2$. Similarly, the Laplace transform of the joint probability density of τ and n is given by

$$\hat{p}(s, n) = \frac{\lambda}{s + \lambda + 2\mathcal{D}} \left(\frac{2\mathcal{D}\hat{\phi}_c(s)}{s + \lambda + 2\mathcal{D}} \right)^n. \quad (3)$$

Therefore, the IET distribution in the frequency domain

is given by

$$\hat{p}(s) = \sum_{n=0}^{\infty} \hat{p}(s, n) = \frac{\lambda}{s + \lambda + 2\mathcal{D}[1 - \hat{\phi}_c(s)]}. \quad (4)$$

Using Eq. (4), we obtain the following expression of the coefficient of variation (CV), defined as the standard deviation divided by the mean, of τ (see Appendix A for the derivation):

$$\text{CV} = \sqrt{1 + \frac{2\lambda\mathcal{D}\hat{\phi}_c''(0)}{[1 - 2\mathcal{D}\hat{\phi}_c'(0)]^2}}, \quad (5)$$

where $\hat{\phi}_c'(0)$ and $\hat{\phi}_c''(0)$ are the first and second derivatives of $\hat{\phi}_c(s)$ evaluated at $s = 0$, respectively.

The asymptotic form of the distribution of first-passage time of random walks in networks with short relaxation time has an exponential tail [65]. With $\phi_c(t) = \alpha e^{-\alpha t}$, which we refer to as the exponential ansatz, Eq. (4) is reduced to

$$\hat{p}(s) = \frac{\lambda(s + \alpha)}{(s + \alpha)(s + \lambda + 2\mathcal{D}) - 2\mathcal{D}\alpha}. \quad (6)$$

The inverse Laplace transform of Eq. (6) is given by

$$\begin{aligned} p(\tau) &= \frac{\lambda}{2\Delta} \left[(\Delta - \lambda - 2\mathcal{D} + \alpha) e^{-\frac{(\lambda+2\mathcal{D}+\alpha-\Delta)\tau}{2}} \right. \\ &\quad \left. + (\Delta + \lambda + 2\mathcal{D} - \alpha) e^{-\frac{(\lambda+2\mathcal{D}+\alpha+\Delta)\tau}{2}} \right], \end{aligned} \quad (7)$$

where $\Delta \equiv \sqrt{(\lambda + 2\mathcal{D} + \alpha)^2 - 4\alpha\lambda} > 0$. Therefore, the distribution of IET is a mixture of two exponential distributions (see Appendix B for a proof). By substituting $\phi_c(t) = \alpha e^{-\alpha t}$ in Eq. (5), we obtain

$$\text{CV}_{\text{ansatz}} = \sqrt{1 + \frac{4\lambda\mathcal{D}}{(2\mathcal{D} + \alpha)^2}}. \quad (8)$$

To mathematically derive the distribution of ICTs, $\phi_c(t)$, we denote by $\vec{s} = (m, n)$ the state of the system in which one walker is in the m th subpopulation and the other walker is in the n th subpopulation. Because the walkers are indistinguishable, the system has $\bar{N} = N(N+1)/2$ states, i.e., (m, n) , where $1 \leq m \leq n \leq N$.

We consider the first-passage time of a continuous-time Markov chain from a state (i, i) , i.e., a copresence, to a state (j, j) , i.e., the next copresence, where $i, j \in \{1, 2, \dots, N\}$. We refer to the states in which the two walkers are in the same subpopulation as absorbing states and those in which the walkers are in different subpopulations as transient states. Let $\mathcal{A} = \{(m, n); m = n\}$ and $\mathcal{B} = \{(m, n); m < n\}$ be the set of absorbing and transient states, respectively. We denote the probability that the dynamics starting in state (i, i) at time 0 is in state $\vec{s} = (m, n)$, where $m \leq n$, at time t by $p_{i,\vec{s}}(t)$, or equivalently, $p_{i,(m,n)}(t)$. We set $\mathbf{p}_i(t) = [\mathbf{p}_i^T(t) \ \mathbf{p}_i^A(t)]$, where $\mathbf{p}_i^T(t) = (p_{i,(1,2)}(t), p_{i,(1,3)}(t), \dots, p_{i,(N-1,N)}(t))$ is the $N_T \equiv N(N-1)/2$ -dimensional vector of the transient states, and $\mathbf{p}_i^A(t) = (p_{i,(1,1)}(t), p_{i,(2,2)}(t), \dots, p_{i,(N,N)}(t))$ is the N -dimensional vector of absorbing states.

At time 0, one of the walkers leaves subpopulation i such that the system leaves the absorbing state (i, i) and enters a transient state. Therefore, the distribution of the initial state of the Markov process is given by $p_{i,(m,n)}(0) = (1 - \delta_{mn})(A_{in}\delta_{mi} + A_{im}\delta_{ni})/k_i^{\text{out}}$, where $k_i^{\text{out}} = \sum_{l=1}^N A_{il}$ is the out-degree of subpopulation i , and δ_{ij} is the Kronecker delta.

The master equation for a transient state $\vec{s} = (m, n)$ is given by

$$\frac{d\mathbf{p}_i^T(t)}{dt} = -\mathbf{p}_i^T(t)L, \quad (9)$$

where $L \equiv 2DI - Q$, matrix Q is the matrix of transitions rates between transient states, and I is the $N_T \times N_T$ identity matrix (see Appendix C for details). Equation (9) leads to

$$\mathbf{p}_i^T(t) = \mathbf{p}_i^T(0)e^{-Lt}. \quad (10)$$

The master equation for the absorbing states is given by

$$\frac{d\mathbf{p}_i^A(t)}{dt} = \mathbf{p}_i^T(t)R, \quad (11)$$

where R is the matrix of transition rates from a transient state to an absorbing state (see Appendix C). By substituting Eq. (10) into Eq. (11), we obtain

$$\mathbf{p}_i^A(t) = \mathbf{p}_i^T(0)L^{-1}(I - e^{-Lt})R. \quad (12)$$

The probability density function of the first-passage time from (i, i) to an absorbing state \vec{s} , denoted by $f_{i,\vec{s}}(t)$, satisfies $p_{i,\vec{s}}^A(t) = \int_0^t f_{i,\vec{s}}^A(t')dt'$. Therefore, the probability density of the first-passage time to the absorbing states is given by

$$\mathbf{f}_i^A(t) = \frac{d\mathbf{p}_i^A(t)}{dt} = \mathbf{p}_i^T(0)e^{-Lt}R, \quad (13)$$

where $\mathbf{f}_i^A(t) = (f_{i1}^A(t), \dots, f_{iN}^A(t))$, and $f_{ij}^A(t)$ is the probability density of the first-passage time from (i, i) to (j, j) .

We define the $N \times N_T$ matrix $P^T(t)$ such that its i th row is given by $\mathbf{p}_i^T(t)$, and the $N \times N$ matrix $F^A(t)$ by $[F^A(t)]_{ij} = f_{ij}^A(t)$. Then, Eq. (13) is equivalent to

$$F^A(t) = P_0^T e^{-Lt} R, \quad (14)$$

where $P_0^T = P^T(0)$.

In the equilibrium, the initial copresence state (i, i) should be the stationary probability of the discrete-time random walk on \mathcal{A} , where the transition probability T_{ij} from (i, i) to (j, j) is given by

$$T_{ij} = \int_0^\infty dt f_{ij}^A(t). \quad (15)$$

Using Eqs. (14) and (15) we obtain the $N \times N$ matrix $[T]_{ij} = T_{ij}$ as

$$T = P_0^T L^{-1} R. \quad (16)$$

We obtain the stationary distribution \mathbf{q}^* for the absorbing states as

$$\mathbf{q}^* T = \mathbf{q}^*, \quad (17)$$

which we can numerically solve for arbitrary networks of subpopulations.

If Q is diagonalizable, we can write

$$e^{Qt} = \sum_{j=1}^{N_T} e^{\gamma_j t} \mathbf{v}_j \mathbf{w}_j, \quad (18)$$

where \mathbf{v}_j and \mathbf{w}_j are the right and left eigenvectors, respectively, associated with eigenvalue γ_j of Q .

By combining Eqs. (14), (17), and (18) we obtain the ICT distribution weighted by the stationary probability of the initial location of the two copresent walkers as

$$\phi_c(t) = \mathbf{q}^* F^A(t) \mathbf{1}_N = \sum_{j=1}^{N_T} c_j \alpha_j e^{-\alpha_j t}, \quad (19)$$

where $c_j = \mathbf{q}^* P_0^T \mathbf{v}_j \mathbf{w}_j \mathbf{1}_{N_T}$, $\alpha_j = 2D - \gamma_j > 0$, and $\mathbf{1}_N$ and $\mathbf{1}_{N_T}$ are the column vectors of size N and N_T , respectively, in which all the elements are 1 (see Appendix D for a proof of Eq. (19) and $\alpha_j > 0$). Because $\sum_{j=1}^{N_T} \mathbf{v}_j \mathbf{w}_j = I$, we have $\sum_{j=1}^{N_T} c_j = 1$. Therefore, $\phi_c(t)$ is a mixture of exponential distributions, including the case in which $c_j < 0$.

By substituting the Laplace transform of Eq. (19) into Eq. (4) and Eq. (5), we obtain

$$\hat{p}(s) = \frac{\lambda}{s + \lambda + 2D[1 - \mathbf{q}^* P_0^T (sI + L)^{-1} R \mathbf{1}_N]} \quad (20)$$

and

$$\text{CV}_{\text{mixture}} = \sqrt{1 + \frac{4\lambda D \mathbf{q}^* P_0^T L^{-1} L^{-1} \mathbf{1}_{N_T}}{(1 + 2D \mathbf{q}^* P_0^T L^{-1} \mathbf{1}_{N_T})^2}}. \quad (21)$$

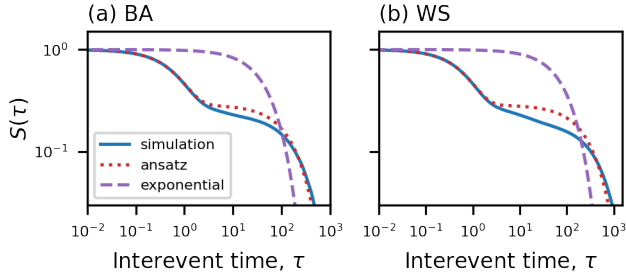


FIG. 2. Survival function of IETs, $S(\tau)$. We show the results for the direct numerical simulation of the model (simulation), the exponential ansatz (ansatz; Eq. (7)), and the single exponential distribution (exponential) whose mean is equal to that for the direct simulations. In Eq. (8), we set $\alpha = 1/\sum_{j=1}^{N_T}(c_j/\alpha_j) = 1/\mathbf{q}^* P_0^T L^{-1} \mathbf{1}_{N_T}$. (a) BA network with $m = 2$. (b) WS network with $p = 0.1$. We set $N = 100$, $\lambda = 1$, and $\mathcal{D} = 0.2$. We stop the simulation when 10^5 events are generated.

This solution depends on the network structure through $\phi_c(t)$.

To compare CV_{ansatz} with CV_{mixture} we impose that the mean ICT is equal between the two. This condition combined with $\phi_c(t) = \alpha e^{-\alpha t}$ and Eq. (19) yields $1/\alpha = \sum_{j=1}^{N_T}(c_j/\alpha_j)$. Then, CV_{mixture} is larger than the CV_{ansatz} because $\sum_m (c_m/\alpha_m^2) > [\sum_m (c_m/\alpha_m)]^2$, which is satisfied by the Sedrakyan's inequality [66]. Therefore, the exponential ansatz, which has led to the mixture of two exponential distributions for IETs, gives a lower bound in terms of the dispersion of IETs. Additionally, in the case of the network of two subpopulations connected to each other, Eq. (19) is reduced to the exponential ansatz (see Appendix D). Therefore, although the time-domain solution of the IET distribution is not available in general, the IETs are guaranteed to be distributed according to a distribution with a heavier tail than a mixture of two exponential distributions.

In fact, if the system starts in state (i, i) and reaches (j, j) to produce an ICT, it restarts from (j, j) to produce the next ICT. Therefore, Eq. (20), which assumes the independence of different ICTs, is only approximate. Nevertheless, the following numerical simulations support that the difference between the approximate solution (i.e., Eqs. (20) and (21)) and the exact solution (see Appendix E) is negligible.

Numerical results—We simulated the model to validate our theory. We show the IET distribution produced by two walkers on the Barabási-Albert (BA) and Watt-Strogatz (WS) networks in Figs. 2(a) and 2(b), respectively. The figure shows that the IET distributions obtained from numerical simulations and ansatz have heavier tails than the exponential distribution whose mean IET is equal to that for the numerical simulations. The distribution obtained from the simulation decays more smoothly than the exponential ansatz.

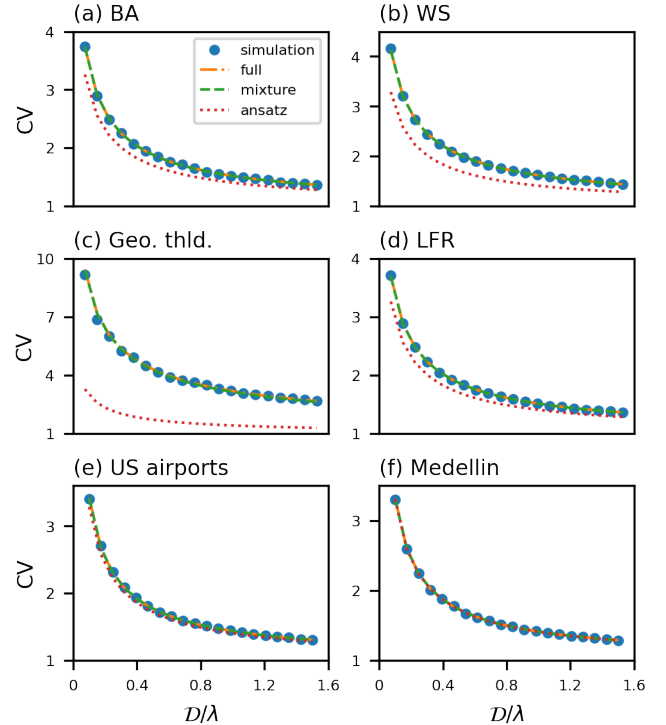


FIG. 3. CV of IET for various metapopulation networks. We compare among the simulation of the model (simulation), the exact theoretical solution (full; see Appendix E), our main theory (mixture; Eq. (21)), and the exponential ansatz (ansatz; Eq. (8)). (a) Barabási-Albert (BA) network with $m = 2$ [67]. (b) Watt-Strogatz (WS) network with $p = 0.1$ [68]. (c) Geographical threshold (Geo. thld.) graph with the threshold value $\theta = 95$, dimension equal to 2, Euclidean distance metric, and probability density function of connecting two nodes that are of distance r given by r^{-2} [69]. (d) Lancichinetti–Fortunato–Radicchi (LFR) model with $\gamma = 3$, $\beta = 1.5$, $\mu = 0.2$, average degree equal to 5, maximum degree equal to 50, and minimum community size equal to 10 [70]. (e) US airport network [71]. (f) Medellin inter-city zone network [72]. In panels (a)–(d), the networks have $N = 100$ nodes. We set $\lambda = 1$.

To be more quantitative and general in terms of the parameter values and variety of networks, we compared the numerically and theoretically obtained CV of IET on six networks. Simultaneously changing λ and \mathcal{D} to $c\lambda$ and $c\mathcal{D}$, where $c > 0$, is equivalent to changing the time from t to ct and using the original λ and \mathcal{D} values. This observation is consistent with our theoretical results for the CV (i.e., Eqs. (8) and (21)), which only depends on \mathcal{D}/λ . Therefore, we set $\lambda = 1$ without loss of generality and varied \mathcal{D} .

The results shown in Fig. 3 indicate that the CV is large when \mathcal{D}/λ is small for all the four model networks and two empirical networks. Moreover, the CV obtained from our theory (Eq. (21) and its fuller version derived in Appendix E) is in an excellent agreement with the numerical results. The exponential ansatz (Eq. (8)) is accu-

rate for the two empirical networks (Figs. 3(e) and 3(f)), reasonably good for two model networks (Figs. 3(a) and 3(d)), and not accurate for the WS and the geographical threshold networks (see Figs. 3(b) and 3(c)). Therefore, spatiality, or the large average path length between nodes, which is present in the last two networks but not in the other networks, may negatively affect the accuracy of the exponential ansatz.

We have assumed simple random walks. More realistic metapopulation models incorporate the recurrent nature of human mobility where individuals iterate between a home subpopulation and a work subpopulation, which are different for different individuals [73–78]. Second-order random walks are another way to better approximate human and animal mobility [79, 80]. Our theory and the result that IETs obey a heavier-tailed distribution than the exponential distribution holds true for a random walk with a commuting pattern between a home node and other nodes (Appendix F) and for second- and higher-order random walks (Appendix G).

Discussion—We have shown that IET distributions are mixtures of exponential distributions for mobile individuals in metapopulation networks. The results hold true under mild conditions, i.e., for various structures of the metapopulation network, a work-home mobility rule, and higher-order random walks. Although a mixture of exponential distributions is technically not heavy-tailed, it often approximates heavy-tailed distributions reasonably well over scales [35, 37, 81]. Therefore, the present results provide a compelling explanation of heavy-tailed IET distributions in human and animal contact data. Additional mechanisms such as circadian or weekly rhythms [33] and dynamics of individuals’ internal states [39] on top of mobility and metapopulation networks may make IET distributions more smooth and more power-law-like.

The present study bridges statistics of IETs and metapopulation models, which have been extensively but in most cases separately investigated topics. For example, heavy-tailed IET distributions suppress epidemic spreading in a majority of scenarios [7–14]. The present results allow a new interpretation of these results. That is, different results of epidemic spreading associated with non-Poissonian IET statistics may owe in large part to whether the structure of the metapopulation network plays a significant role (which would yield heavier-tailed IET distributions) or the population is sufficiently well-mixed (which would yield an exponential IET distribution). The effects of IET statistics other than their heavy-tailed distributions [2, 3, 82] on epidemic and other dynamical processes may also be due to the underlying metapopulation network. Reexamining the role of IETs in contagion and other dynamical processes from the viewpoint of metapopulation networks warrants future work.

EFdR thanks the financial support by the Coordenação de Aperfeiçoamento de Pessoal de Nível Superior - Brasil (CAPES) - Finance Code 001. NM thanks the financial support by AFOSR European Office (under

Grant no. FA9550-19-1-7024), the Nakatani Foundation, and the Sumitomo Foundation.

Appendix A: Coefficient of variation

The coefficient of variation (CV) is defined as

$$\text{CV} = \sqrt{\frac{\langle \tau^2 \rangle}{\langle \tau \rangle^2} - 1}, \quad (\text{A1})$$

where $\langle \cdot \rangle$ is the expectation. From Eq. (4), we obtain the first and second moments of τ as

$$\langle \tau \rangle = - \left. \frac{d\hat{p}(s)}{ds} \right|_{s=0} = \frac{1}{\lambda} \left(1 - 2\mathcal{D} \frac{d\hat{\phi}_c(0)}{ds} \right) \quad (\text{A2})$$

and

$$\begin{aligned} \langle \tau^2 \rangle &= \left. \frac{d^2\hat{p}(s)}{ds^2} \right|_{s=0} \\ &= \frac{2\mathcal{D}}{\lambda} \frac{d^2\hat{\phi}_c(0)}{ds^2} + \frac{1}{\lambda^2} \left(1 - 2\mathcal{D} \frac{d\hat{\phi}_c(0)}{ds} \right)^2. \end{aligned} \quad (\text{A3})$$

Appendix B: Distribution of IET with the exponential ansatz

In this section we show that Eq. (7) is a mixture of two exponential distributions. We first rewrite Eq. (7) as

$$\begin{aligned} p(\tau) &= C_1 \left(\frac{\lambda + 2\mathcal{D} + \alpha - \Delta}{2} \right) e^{-\frac{(\lambda + 2\mathcal{D} + \alpha - \Delta)\tau}{2}} \\ &\quad + C_2 \left(\frac{\lambda + 2\mathcal{D} + \alpha + \Delta}{2} \right) e^{-\frac{(\lambda + 2\mathcal{D} + \alpha + \Delta)\tau}{2}}, \end{aligned} \quad (\text{B1})$$

where

$$C_1 = \frac{\lambda(\Delta - \lambda - 2\mathcal{D} + \alpha)}{\Delta(\lambda + 2\mathcal{D} + \alpha - \Delta)} \quad (\text{B2})$$

and

$$C_2 = \frac{\lambda(\Delta + \lambda + 2\mathcal{D} - \alpha)}{\Delta(\lambda + 2\mathcal{D} + \alpha + \Delta)}. \quad (\text{B3})$$

The two exponents in Eq. (B1) are positive because

$$0 < \Delta = \sqrt{(\lambda + 2\mathcal{D} + \alpha)^2 - 4\alpha\lambda} < \lambda + 2\mathcal{D} + \alpha. \quad (\text{B4})$$

Because

$$\Delta - (\lambda + 2\mathcal{D} - \alpha)^2 = 8\lambda\mathcal{D} > 0, \quad (\text{B5})$$

which imply that

$$\Delta > \pm(\lambda + 2\mathcal{D} - \alpha), \quad (\text{B6})$$

the weights C_1 and C_2 are positive. Equations (B2) and (B3) also imply that

$$C_1 + C_2 = 1. \quad (\text{B7})$$

Therefore, Eq. (B1) is a mixture of two exponential distributions.

Appendix C: Transition rate matrix

An element of the transition rate matrix W from a state $\vec{s} = (m, n)$ to a state $\vec{s}' = (m', n')$ is given by

$$W_{\vec{s}\vec{s}'} = (1 - \delta_{mn})(1 - \delta_{m'n'}) \left[\frac{\mathcal{D}}{k_m} (A_{mm'}\delta_{nn'} + A_{mn'}\delta_{nm'}) + \frac{\mathcal{D}}{k_n} (A_{nn'}\delta_{mm'} + A_{nm'}\delta_{mn'}) \right] \\ + (1 - \delta_{mn})\delta_{m'n'} \left[\frac{\mathcal{D}}{k_m} A_{mm'}\delta_{nn'} + \frac{\mathcal{D}}{k_n} A_{nn'}\delta_{mm'} \right]. \quad (\text{C1})$$

The first term on the right-hand side of Eq. (C1) represents the transitions between transient states. We define Q as the $N_T \times N_T$ matrix of transition rates between transient states, i.e., $W_{\vec{s}\vec{s}'} = Q_{\vec{s}\vec{s}'}$, where $\vec{s} \in \mathcal{B}$ and $\vec{s}' \in \mathcal{B}$. Then,

$$Q_{\vec{s}\vec{s}'} = \frac{\mathcal{D}}{k_m} (A_{mm'}\delta_{nn'} + A_{mn'}\delta_{nm'}) \\ + \frac{\mathcal{D}}{k_n} (A_{nn'}\delta_{mm'} + A_{nm'}\delta_{mn'}). \quad (\text{C2})$$

The second term on the right-hand side of Eq. (C1) represents the transitions from a transient state to an absorbing state. We define R as the $N_T \times N$ matrix of transition rates from a transient state to an absorbing state, i.e., $W_{\vec{s}\vec{s}'} = R_{\vec{s}\vec{s}'}$, where $\vec{s} \in \mathcal{B}$ and $\vec{s}' \in \mathcal{A}$. Then,

$$R_{\vec{s}\vec{s}'} = \frac{\mathcal{D}}{k_m} A_{mm'}\delta_{nn'} + \frac{\mathcal{D}}{k_n} A_{nn'}\delta_{mm'}. \quad (\text{C3})$$

Note that

$$\sum_{\vec{s}'} W_{\vec{s}\vec{s}'} = \sum_{\vec{s}' \in \mathcal{B}} Q_{\vec{s}\vec{s}'} + \sum_{\vec{s}' \in \mathcal{A}} R_{\vec{s}\vec{s}'} = 2\mathcal{D} \quad (\text{C4})$$

for any $\vec{s} \in \mathcal{B}$. Equation (C4) represents the fact that the system leaves any transient state at rate $2\mathcal{D}$ owing to the movement of each walker, which occurs at rate \mathcal{D} .

The master equation for a transient state $\vec{s} = (m, n)$, which is equivalent to Eq. (9) in the main text, is given by

$$\frac{dp_{i,\vec{s}}^T(t)}{dt} = \sum_{\vec{s}' \in \mathcal{B}} [p_{i,\vec{s}'}^T(t)Q_{\vec{s}'\vec{s}} - p_{i,\vec{s}}^T(t)Q_{\vec{s}\vec{s}'}] \\ - \sum_{\vec{s}' \in \mathcal{A}} p_{i,\vec{s}}^T(t)R_{\vec{s}\vec{s}'} \\ = -2\mathcal{D}p_{i,\vec{s}}(t) + \sum_{\vec{s}' \in \mathcal{B}} p_{i,\vec{s}'}(t)Q_{\vec{s}'\vec{s}}. \quad (\text{C5})$$

In Eq. (C5), we used the fact that the sum of transition rates from any transient state to other states is equal to $2\mathcal{D}$, as shown in Eq.(C4).

Appendix D: Distribution of ICTs

To derive the ICT distribution, we first note that Eq. (C4) leads to

$$R\mathbf{1}_N = L\mathbf{1}_{N_T}. \quad (\text{D1})$$

Then, by combining Eqs. (14), (17), and (D1), we obtain

$$\phi_c(t) = \mathbf{q}^* F^A(t) \mathbf{1}_N \\ = \mathbf{q}^* P_0^T e^{-Lt} R \mathbf{1}_N \\ = e^{-2\mathcal{D}t} \mathbf{q}^* P_0^T (2\mathcal{D}I - Q) e^{Qt} \mathbf{1}_{N_T}. \quad (\text{D2})$$

By substituting Eq. (18) into Eq. (D2), we find

$$\phi_c(t) = \sum_{j=1}^{N_T} \mathbf{q}^* P_0^T \mathbf{v}_j \mathbf{w}_j \mathbf{1}_{N_T} (2\mathcal{D} - \gamma_j) e^{-(2\mathcal{D} - \gamma_j)t} \\ = \sum_{j=1}^{N_T} c_j \alpha_j e^{-\alpha_j t}. \quad (\text{D3})$$

In our model, all transient states are reachable from any transient state. Therefore, Q is irreducible and, by definition, non-negative. Hence, by the Perron-Frobenius theorem, the spectral radius of Q , $\rho(Q)$, satisfies $\rho(Q) \leq \max_{\vec{s}} \sum_{\vec{s}' \in \mathcal{B}} Q_{\vec{s}\vec{s}'}$. Using Eq. (C4) we obtain $\rho(Q) \leq 2\mathcal{D}$, which implies that $2\mathcal{D} - \gamma_j \geq 0$, for all j .

In the particular case of two subpopulations connected to each other ($N = 2$), the number of transient states is $N_T = 1$. Therefore, Eq. (D3) becomes

$$\phi_c(t) = \alpha_1 e^{-\alpha_1 t}, \quad (\text{D4})$$

which is equivalent to the exponential ansatz. In this case, there is one transient state and two absorbing states. Therefore, $Q = 0$, $R = [\mathcal{D} \ \mathcal{D}]$, $L^{-1} = 1/2\mathcal{D}$, and $\mathbf{1}_{N_T} = 1$. From Eq. (16) we obtain

$$T = P_0^T L^{-1} R = \frac{1}{2} \begin{bmatrix} 1 & 1 \\ 1 & 1 \end{bmatrix}, \quad (\text{D5})$$

such that $\mathbf{q}^* = [1/2 \ 1/2]$. Then, we obtain α_1 as

$$\alpha_1 = \frac{1}{\mathbf{q}^* P_0^T L^{-1} \mathbf{1}_{N_T}} = 2\mathcal{D}. \quad (\text{D6})$$

Therefore, for two subpopulations the ICT distribution is given by

$$\phi_c(t) = 2\mathcal{D}e^{-2\mathcal{D}t}. \quad (\text{D7})$$

Appendix E: Exact solution for the IET distribution

In this section we derive the exact solution for the IET distribution. The probability density with which the two walkers are copresent in subpopulation j after time t given that the last copresence terminated at

time 0 in subpopulation i is given by $f_{ij}^A(t)$, which is given via Eq. (14). In other words, $f_{ij}^A(t)$ is the probability density of an ICT, t , from (i, i) to (j, j) . Note that $f_{ij}^A(t) = \phi_c(j, t|i)$ and the normalization is given by $\sum_{j=1}^N \int_0^\infty dt f_{ij}^A(t) = 1$. We denote by $p_{ij}(\tau, n)$ the joint distribution of an IET, τ , and the number of copresences, n , such that the event has occurred in subpopulation i and the next event occurs in subpopulation j . The normalization is given by $\sum_{j=0}^N \sum_{n=0}^\infty \int_0^\infty d\tau p_{ij}(\tau, n) = 1$. We derive the Laplace transform of $p_{ij}(\tau, n)$ by extending Eq. (3) as follows:

$$\hat{p}_{ij}(s, n) = \frac{\lambda(2\mathcal{D})^n}{(s + \lambda + 2\mathcal{D})^{n+1}} \sum_{l_1=1}^N \sum_{l_2=1}^N \cdots \sum_{l_{n-1}=1}^N \hat{\phi}_c(l_1, s|i) \hat{\phi}_c(l_2, s|l_1) \cdots \hat{\phi}_c(j, s|l_{n-1}). \quad (\text{E1})$$

We define the $N \times N$ matrix $\hat{\Phi}(s)$ by $[\hat{\Phi}(s)]_{ij} = \hat{\phi}_c(j, s|i)$. Using Eq. (14), we obtain

$$\hat{\Phi}(s) = P_0^T (sI + L)^{-1} R. \quad (\text{E2})$$

We also define the $N \times N$ matrix $\hat{\Pi}(s, n)$ by $[\hat{\Pi}(s, n)]_{ij} = \hat{p}_{ij}(s, n)$. Using Eq. (E1), we obtain

$$\begin{aligned} \hat{\Pi}(s) &\equiv \sum_{n=0}^{\infty} \hat{\Pi}(s, n) \\ &= \frac{\lambda}{s + \lambda + 2\mathcal{D}} \sum_{n=0}^{\infty} \left[\frac{2\mathcal{D}\hat{\Phi}(s)}{s + \lambda + 2\mathcal{D}} \right]^n \\ &= \lambda \left\{ (s + \lambda)I + 2\mathcal{D} \left[I - \hat{\Phi}(s) \right] \right\}^{-1}. \end{aligned} \quad (\text{E3})$$

We denote by $\hat{g}(s)$ the stationary distribution in the frequency domain of IET weighted by the stationary probability of the initial location of the two copresent walkers. By combining Eqs. (E2), and (E3), we obtain

$$\begin{aligned} \hat{g}(s) &= \mathbf{q}^* \hat{\Pi}(s) \mathbf{1}_N \\ &= \lambda \mathbf{q}^* \left\{ (s + \lambda)I + 2\mathcal{D} \left[I - P_0^T (sI + L)^{-1} R \right] \right\}^{-1} \mathbf{1}_N, \end{aligned} \quad (\text{E4})$$

where \mathbf{q}^* is given by (17).

With Eq. (E4), the first and second moments of IET from are given by

$$\langle \tau \rangle = \frac{1}{\lambda} \left(1 + 2\mathcal{D} \mathbf{q}^* \hat{\Pi}(0) P_0^T L^{-1} \mathbf{1}_{N_T} \right) \quad (\text{E5})$$

and

$$\langle \tau^2 \rangle = \frac{4\mathcal{D}}{\lambda} \mathbf{q}^* \hat{\Pi}(0) P_0^T L^{-2} \mathbf{1}_{N_T} + \frac{2}{\lambda^2} \mathbf{q}^* \left(\hat{\Pi}(0) + 2\mathcal{D} \hat{\Pi}(0) P_0^T L^{-2} R \right)^2 \mathbf{1}_N, \quad (\text{E6})$$

respectively, where

$$\hat{\Pi}(0) = \lambda \left[(\lambda + 2\mathcal{D})I - 2\mathcal{D} P_0^T L^{-1} R \right]^{-1}. \quad (\text{E7})$$

By substituting Eqs. (E5) and (E6) into Eq. (A1), we obtain

$$\text{CV} = \sqrt{\frac{4\lambda\mathcal{D}\mathbf{q}^* \hat{\Pi}(0) P_0^T L^{-2} \mathbf{1}_{N_T} + 2\mathbf{q}^* \left(\hat{\Pi}(0) + 2\mathcal{D} \hat{\Pi}(0) P_0^T L^{-2} R \right)^2 \mathbf{1}_N}{\left(1 + 2\mathcal{D} \mathbf{q}^* \hat{\Pi}(0) P_0^T L^{-1} \mathbf{1}_{N_T} \right)^2}} - 1. \quad (\text{E8})$$

Appendix F: Work-home model

In this section, we analyze the IET distribution for a mobility rule that mimics a daily commuting pattern between home and other places, such as work [73–78].

We emulate this situation by assigning to each walker a home subpopulation and allowing it to visit subpopulations adjacent to the home subpopulation. Then, each walker is confined to a star graph of which the central subpopulation is the home subpopulation and the leaves are other locations such as work. Without loss of generality, we consider two random walkers on the respective star graphs to generate sequences of IETs.

We examine two cases. In the first case, the two walkers share the home subpopulation and all leaf subpopulations, as shown in Fig. 4(a). In other words, the two walkers are confined to the same star graph, and events between them may occur in any subpopulation. Therefore, our theory directly applies.

In the second case, we assume that the two walkers have different home subpopulations and share some but not necessarily all the leaf subpopulations, as shown in Fig. 4(b). This case mimics, for example, the situation in which the two individuals are coworkers living in different cities. Events may occur between the walkers only when they are copresent in any of the shared leaf subpopulations. To derive the states and the transition rates between the states, we distinguish the two walkers and the subpopulations. There are three types of subpopula-

tions: the home subpopulations, which are unshared, the shared leaf subpopulations, which are work locations, for example, and the unshared leaf subpopulations, which represent other locations that one but not both walkers visits. In a network with N subpopulations, two subpopulations are home subpopulations, N_s subpopulations are the shared leaf subpopulations, and walkers 1 and 2 have N_1 and N_2 unshared leaf subpopulations, respectively, such that $N = 2 + N_s + N_1 + N_2$.

We define the home subpopulation nodes by h_1 and h_2 , and the set of shared leaf subpopulations by $\mathcal{W} = \{w_1, w_2, \dots, w_{N_s}\}$. There are four types of transient states. In the first type of transient states, both walkers are in different shared leaf subpopulations. There are $N_s(N_s - 1)$ such states. In the second type, walker 1 is in a shared leaf subpopulation, and walker 2 is not. There are $N_s(N_1 + 1)$ such states. In the third type, walker 2 is in a shared leaf subpopulation, and walker 1 is not. There are $N_s(N_2 + 1)$ such states. In the fourth type, both walkers are not in any of the shared leaf subpopulations. There are $(N_1 + 1)(N_2 + 1)$ such states. Therefore, there are

$$N_T = N_s(N_s - 1) + N_s(N_1 + N_2 + 2) + (N_1 + 1)(N_2 + 1) \quad (\text{F1})$$

transient states in total. Each element of the $N_T \times N_T$ matrix of transition rates between transient states, $Q_{\vec{s}\vec{s}'}$, where $\vec{s} = (m_1, m_2) \in \mathcal{B}$ and $\vec{s}' = (m'_1, m'_2) \in \mathcal{B}$, is given by

$$\begin{aligned} Q_{\vec{s}\vec{s}'} &= \chi_{\mathcal{W}}(m_1)\chi_{\mathcal{W}}(m_2) (\mathcal{D}A_{m_1, m'_1} \delta_{m'_1, h_1} \delta_{m_2, m'_2} + \mathcal{D}A_{m_2, m'_2} \delta_{m'_2, h_2} \delta_{m_1, m'_1}) \\ &+ \chi_{\mathcal{W}}(m_1)[1 - \chi_{\mathcal{W}}(m_2)] \left(\mathcal{D}A_{m_1, m'_1} \delta_{m'_1, h_1} \delta_{m_2, m'_2} + \frac{\mathcal{D}}{k_{m_2}} A_{m_2, m'_2} \delta_{m_1, m'_1} \right) \\ &+ \chi_{\mathcal{W}}(m_2)[1 - \chi_{\mathcal{W}}(m_1)] \left(\frac{\mathcal{D}}{k_{m_1}} A_{m_1, m'_1} \delta_{m_2, m'_2} + \mathcal{D}A_{m_2, m'_2} \delta_{m'_2, h_2} \delta_{m_1, m'_1} \right) \\ &+ [1 - \chi_{\mathcal{W}}(m_1)][1 - \chi_{\mathcal{W}}(m_2)] \left(\frac{\mathcal{D}}{k_{m_1}} A_{m_1, m'_1} \delta_{m_2, m'_2} + \frac{\mathcal{D}}{k_{m_2}} A_{m_2, m'_2} \delta_{m_1, m'_1} \right), \end{aligned} \quad (\text{F2})$$

where $\chi_{\mathcal{W}}$ is the indicator function defined by

$$\chi_{\mathcal{W}}(m) = \begin{cases} 1 & \text{if } m \in \mathcal{W}, \\ 0 & \text{if } m \notin \mathcal{W}. \end{cases} \quad (\text{F3})$$

In an absorbing state, the two walkers are copresent in one of the shared leaf subpopulations. Therefore, there are N_s absorbing states. Each element of the $N_T \times N_w$ matrix of transition rates from a transient state to an absorbing state, $R_{\vec{s}\vec{s}'}$, where $\vec{s} = (m_1, m_2) \in \mathcal{B}$ and $\vec{s}' =$

$(m'_1, m'_2) \in \mathcal{A}$, is given by

$$\begin{aligned} R_{\vec{s}\vec{s}'} &= \chi_{\mathcal{W}}(m_1)[1 - \chi_{\mathcal{W}}(m_2)] \frac{\mathcal{D}}{k_{m_2}} A_{m_2, m'_1} \delta_{m_1, m'_1} \\ &+ \chi_{\mathcal{W}}(m_2)[1 - \chi_{\mathcal{W}}(m_1)] \frac{\mathcal{D}}{k_{m_1}} A_{m_1, m'_2} \delta_{m_2, m'_2}. \end{aligned} \quad (\text{F4})$$

The distribution of the initial state of the Markov process, is given by

$$\begin{aligned} p_{i, (m_1, m_2)}(0) &= \frac{1}{2} (1 - \delta_{m_1, m_2}) (A_{i, m_1} \delta_{m_1, h_1} \delta_{m_2, i} \\ &+ A_{i, m_2} \delta_{m_2, h_2} \delta_{m_1, i}). \end{aligned} \quad (\text{F5})$$

Then, with Eqs. (F2), (F4), and (F5) as inputs to our theory, the calculation steps to derive the distribution and CV of IET remain the same.

The CV values obtained from the simulation and the theory for the case in which the two walkers share the home and the case in which they have different homes are shown in Figs. 4(c) and 4(d), respectively. In both cases, the results are similar to those shown in Fig. 3, i.e., the CV is large when \mathcal{D}/λ is small, and the theory agrees with the simulation. The exponential ansatz solution yields slightly smaller values of CV than the numerical simulations, which we also observe in Fig. 3.

Appendix G: Higher-order random walks

In this section, we show that our theory holds true when the individuals move according to higher-order random walks. We focus on second-order random walks and then explain how our theory generalizes to higher orders.

In a second-order random walk, the probability with which a walker visits the next node depends on its current and last visited nodes [79, 80]. Therefore, the state of a single walker is defined by a pair of nodes (m_-, m) , where m is the currently visited node, and m_- is the node that the walker visited just before arriving in m . It should be noted that $m \neq m_-$ and that we distinguish between (m_-, m) and (m, m_-) . In other words, the state of each walker is specified by a directed edge. For example, the sequence of a walker's positions from node i to j and then to k is given by $(i, j) \rightarrow (j, k)$. Therefore, in a second-order random walk, we can regard the movement of the walkers as a first-order random walk from directed edge (i, j) to directed edge (j, k) instead of between nodes. We assume in the following text that there are N subpopulations and M undirected edges. Then, a walker moves among $2M$ directed edges.

The state of the system of two second-order random walkers is defined by a pair of directed edges, one for each walker. For example, if one walker is currently in subpopulation m and the other walker in subpopulation n , we denote the state of the system by $((m_-, m), (n_-, n))$. Because the walkers are indistinguishable the system has $\bar{N} = 2M(2M + 1)/2 = M(2M + 1)$ states in total.

We denote the next state of the system by $((m'_-, m'), (n'_-, n'))$ and suppose that the walker at subpopulation m has moved to subpopulation m_{new} . Therefore, the new state $((m'_-, m'), (n'_-, n'))$ is equal to $((m, m_{\text{new}}), (n_-, n))$. If $m_{\text{new}} = n$, then the next state (i.e., $((m'_-, m'), (n'_-, n'))$) is an absorbing state. Otherwise, it is a transient state.

The number of absorbing states with which the two walkers meet at node i is given by $k_i + \binom{k_i}{2} = k_i(k_i + 1)/2$, where k_i is the degree of node i . Note that $((j, i), (j, i))$, where j is a neighbor of i , is also a valid absorbing state. Then, the system has $N_A = \sum_{i=1}^N k_i(k_i + 1)/2 = M + \frac{1}{2} \sum_{i=1}^N k_i^2$ absorbing states. The number of transient states is given by $N_T = \bar{N} - N_A = 2M^2 - \frac{1}{2} \sum_{i=1}^N k_i^2$.

Because we have identified all the transient states, absorbing states, and state transition rules, one is able to define the $N_T \times N_T$ matrix Q of transition rates between transient states and the $N_T \times N_A$ matrix R of transition rates from a transient state to an absorbing state. Then, the theory that follows is the same as the one developed in the main text and Appendix E.

It is straightforward to extend the same procedure to the case of directed metapopulation networks and higher-order (i.e., third-order or higher) random walks. For a third-order random walk, for instance, the state of the system is described by a pair of triples, i.e., $((m_{-2}, m_{-1}, m), (n_{-2}, n_{-1}, n))$, where m is the subpopulation that the first walker currently visits, m_{-1} is the node that the same walker visited just before m , m_{-2} is the subpopulation that the walker visited just before m_{-1} , and analogous for (n_{-2}, n_{-1}, n) .

As an example of a second-order random walk, we simulated the non-backtracking random walk. By definition, a non-backtracking random walker on an undirected unweighted network that has moved from m_- to m , moves to any of the neighbors except m_- with the equal probability in the next move [83, 84]. The CV of IET for two non-backtracking random walkers on various networks is shown in Fig. 5. The results are similar to those for the simple random walk shown in Fig. 3. In other words, the CV is substantially larger than 1 and large when \mathcal{D}/λ is small. In general, the CV values for the non-backtracking random walk are somewhat smaller than those for the simple random walk.

-
- [1] P. Holme and J. Saramäki, Temporal networks, *Phys. Rep.* **519**, 97 (2012).
- [2] N. Masuda and R. Lambiotte, *A Guide to Temporal Networks*, 2nd ed. (World Scientific, Singapore, 2020).
- [3] M. Karsai, H.-H. Jo, and K. Kaski, *Bursty Human Dynamics* (Springer, Berlin, 2018).
- [4] P. Holme and J. Saramäki, *Temporal Network Theory* (Springer, Cham, 2019).
- [5] A.-L. Barabási, The origin of bursts and heavy tails in human dynamics, *Nature* **435**, 207 (2005).
- [6] A. Vázquez *et al.*, Modeling bursts and heavy tails in human dynamics, *Phys. Rev. E* **73**, 036127 (2006).
- [7] B. Min, K.-I. Goh, and A. Vázquez, Spreading dynamics following bursty human activity patterns, *Phys. Rev. E* **83**, 036102 (2011).
- [8] M. Karsai, M. Kivelä, R. K. Pan, K. Kaski, J. Kertész, A.-L. Barabási, and J. Saramäki, Small but slow world: How network topology and burstiness slow down spreading, *Phys. Rev. E* **83**, 025102(R) (2011).
- [9] L. E. C. Rocha, F. Liljeros, and P. Holme, Simulated epidemics in an empirical spatiotemporal network of 50,185 sexual contacts, *PLoS Comput. Biol.* **7**, e1001109 (2011).

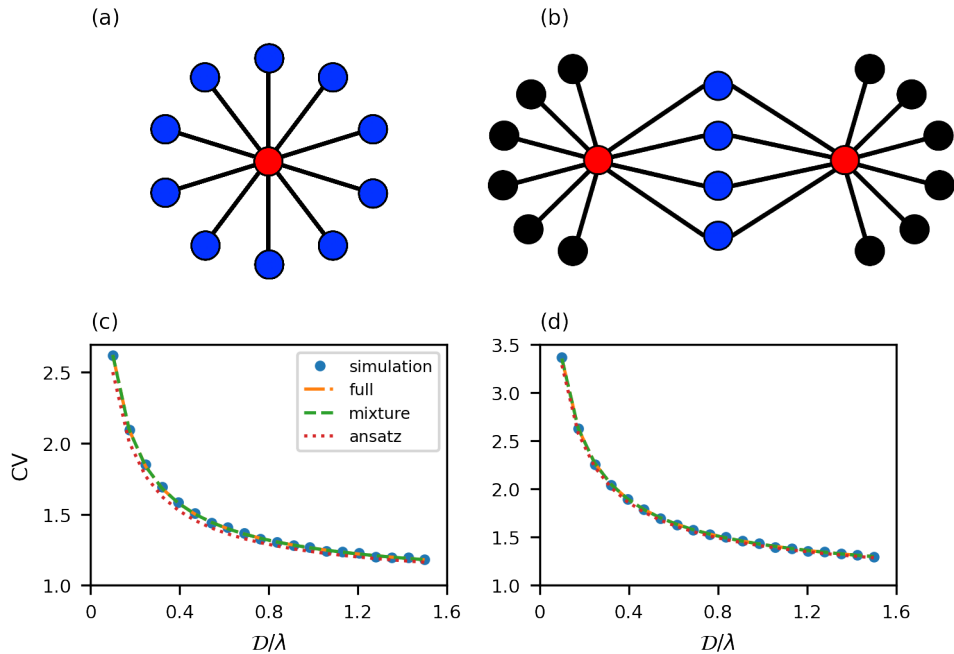


FIG. 4. CV of IET under recurrent mobility patterns. Two situations that mimic the recurrent human mobility pattern of commuting between home and other places. In the star graph shown in panel (a), the two walkers share the home subpopulation, shown in red, and all the leaf subpopulations, shown in blue. In the situation shown in panel (b), the walkers have different home subpopulations, share some leaf subpopulations (shown in blue) but not others (shown in black). We compare the CV of IET among the simulation of the model (simulation), the exact solution (full) from Eq. (E8), the mixture of exponential distribution solution (mixture) from Eq. (21), and the exponential ansatz solution (ansatz) from Eq. (8) in (c) and (d) for the metapopulation network and the mobility rule shown in (a) and (b), respectively. We set $\lambda = 1$.

- [10] G. Miritello, E. Moro, and R. Lara, Dynamical strength of social ties in information spreading, *Phys. Rev. E* **83**, 045102(R) (2011).
- [11] N. Masuda and P. Holme, Predicting and controlling infectious disease epidemics using temporal networks, *F1000Prime Rep.* **5**, 6 (2013).
- [12] H.-H. Jo, J. I. Perotti, K. Kaski, and J. Kertész, Analytically solvable model of spreading dynamics with non-poissonian processes, *Phys. Rev. X* **4**, 011041 (2014).
- [13] R. Pastor-Satorras, C. Castellano, P. Van Mieghem, and A. Vespignani, Epidemic processes in complex networks, *Rev. Mod. Phys.* **87**, 925 (2015).
- [14] N. Masuda and P. Holme, *Temporal Network Epidemiology* (Springer, Berlin, 2017).
- [15] Y. Wu, C. Zhou, M. Chen, J. Xiao, and J. Kurths, Human comment dynamics in on-line social systems, *Physica A* **389**, 5832 (2010).
- [16] T. Takaguchi and N. Masuda, Voter model with non-poissonian interevent intervals, *Phys. Rev. E* **84**, 036115 (2011).
- [17] J. Fernández-Gracia, V. M. Eguíluz, and M. San Miguel, Update rules and interevent time distributions: Slow ordering versus no ordering in the voter model, *Phys. Rev. E* **84**, 015103(R) (2011).
- [18] R. Nishi and N. Masuda, Dynamics of social balance under temporal interaction, *EPL* **107**, 48003 (2014).
- [19] A. Li, L. Zhou, Q. Su, S. P. Cornelius, Y.-Y. Liu, L. Wang, and S. A. Levin, Evolution of cooperation on temporal networks, *Nat. Commun.* **11**, 2259 (2020).
- [20] F. Karimi and P. Holme, Threshold model of cascades in empirical temporal networks, *Physica A* **392**, 3476 (2013).
- [21] T. Takaguchi, N. Masuda, and P. Holme, Bursty communication patterns facilitate spreading in a threshold-based epidemic dynamics, *PLoS ONE* **8**, e68629 (2013).
- [22] V.-P. Backlund, J. Saramäki, and R. K. Pan, Effects of temporal correlations on cascades: Threshold models on temporal networks, *Phys. Rev. E* **89**, 062815 (2014).
- [23] S. Unicomb, G. Iñiguez, J. P. Gleeson, and M. Karsai, Dynamics of cascades on burstiness-controlled temporal networks, *Nat. Commun.* **12**, 133 (2021).
- [24] T. Hoffmann, M. A. Porter, and R. Lambiotte, Generalized master equations for non-poisson dynamics on networks, *Phys. Rev. E* **86**, 046102 (2012).
- [25] M. Starnini, A. Baronchelli, A. Barrat, and R. Pastor-Satorras, Random walks on temporal networks, *Phys. Rev. E* **85**, 056115 (2012).
- [26] L. Speidel, R. Lambiotte, K. Aihara, and N. Masuda, Steady state and mean recurrence time for random walks on stochastic temporal networks, *Phys. Rev. E* **91**, 012806 (2015).
- [27] N. Masuda, M. A. Porter, and R. Lambiotte, Random walks and diffusion on networks, *Phys. Rep.* **716**, 1 (2017).
- [28] A. Vázquez, Exact results for the Barabási model of human dynamics, *Phys. Rev. Lett.* **95**, 248701 (2005).
- [29] G. Grinstein and R. Linsker, Biased diffusion and universality in model queues, *Phys. Rev. Lett.* **97**, 130201 (2006).

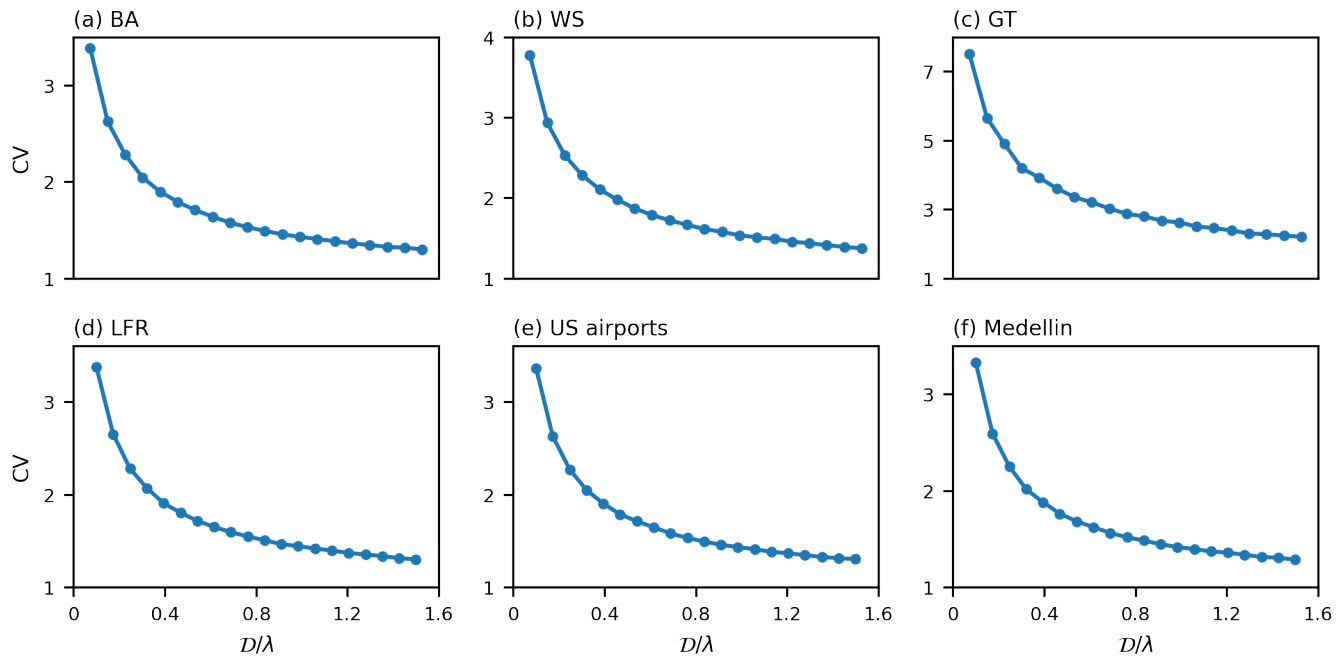


FIG. 5. CV of IET obtained from the simulation of two non-backtracking random walkers for various metapopulation networks. (a) Barabási-Albert (BA) network with $m = 2$. (b) Watt-Strogatz (WS) network with $p = 0.1$. (c) Geographical threshold graph with threshold value $\theta = 95$, dimension equal to 2, Euclidean distance metric, and probability density function of connecting two nodes that are of distance r given by r^{-2} . (d) Lancichinetti–Fortunato–Radicchi (LFR) model with $\gamma = 3$, $\beta = 1.5$, $\mu = 0.2$, average degree equal to 5, maximum degree equal to 50, and minimum community size equal to 10. (e) US airport network. (f) Medellin inter-city zones. In panels (a)–(d), the networks have $N = 100$ nodes. We set $\lambda = 1$.

- (2006).
- [30] N. Masuda, J. S. Kim, and B. Kahng, Priority queues with bursty arrivals of incoming tasks, *Phys. Rev. E* **79**, 036106 (2009).
- [31] J. G. Oliveira and A. Vázquez, Impact of interactions on human dynamics, *Physica A* **388**, 187 (2009).
- [32] H.-H. Jo, R. K. Pan, and K. Kaski, Time-varying priority queuing models for human dynamics, *Phys. Rev. E* **85**, 066101 (2012).
- [33] R. D. Malmgren, D. B. Stouffer, A. E. Motter, and L. A. N. Amaral, A poissonian explanation for heavy tails in e-mail communication, *Proc. Natl. Acad. Sci. U.S.A.* **105**, 18153 (2008).
- [34] R. D. Malmgren, D. B. Stouffer, A. S. L. O. Campanharo, and L. A. N. Amaral, On universality in human correspondence activity, *Science* **325**, 1696 (2009).
- [35] N. Masuda, T. Takaguchi, N. Sato, and K. Yano, Self-exciting point process modeling of conversation event sequences, in *Temporal Networks*, edited by P. Holme and J. Saramäki (Springer, Berlin, 2013) p. 245.
- [36] N. Masuda and P. Holme, Small inter-event times govern epidemic spreading on networks, *Phys. Rev. Res.* **2**, 023163 (2020).
- [37] M. Okada, K. Yamanishi, and N. Masuda, Long-tailed distributions of inter-event times as mixtures of exponential distributions, *R. Soc. Open Sci.* **7**, 191643 (2020).
- [38] Z.-Q. Jiang, W.-J. Xie, M.-X. Li, W.-X. Zhou, and D. Sornette, Two-state markov-chain poisson nature of individual cellphone call statistics, *J. Stat. Mech.* (2016) 073210.
- [39] E. Fonseca dos Reis, A. Li, and N. Masuda, Generative models of simultaneously heavy-tailed distributions of interevent times on nodes and edges, *Phys. Rev. E* **102**, 052303 (2020).
- [40] T. Takaguchi, M. Nakamura, N. Sato, K. Yano, and N. Masuda, Predictability of conversation partners, *Phys. Rev. X* **1**, 011008 (2011).
- [41] A. Panisson, A. Barrat, C. Cattuto, W. Van den Broeck, G. Ruffo, and R. Schifanella, On the dynamics of human proximity for data diffusion in ad-hoc networks, *Ad Hoc Networks* **10**, 1532 (2012).
- [42] A. Panisson, L. Gauvin, A. Barrat, and C. Cattuto, Fingerprinting temporal networks of close-range human proximity, in *2013 IEEE International Conference on Pervasive Computing and Communications Workshops (PERCOM Workshops)* (2013) p. 261.
- [43] A. Barrat and C. Cattuto, Temporal networks of face-to-face human interactions, in *Temporal Networks*, edited by P. Holme and J. Saramäki (Springer, Berlin, 2013) p. 191.
- [44] L. Gauvin, A. Panisson, C. Cattuto, and A. Barrat, Activity clocks: Spreading dynamics on temporal networks of human contact, *Sci. Rep.* **3**, 3099 (2013).
- [45] J. Fournet and A. Barrat, Contact patterns among high school students, *PLoS ONE* **9**, e107878 (2014).
- [46] C. L. Vestergaard, M. Génois, and A. Barrat, How memory generates heterogeneous dynamics in temporal networks, *Phys. Rev. E* **90**, 042805 (2014).
- [47] M. Génois and A. Barrat, Can co-location be used as a proxy for face-to-face contacts?, *EPJ Data Sci.* **7**, 11

- (2018).
- [48] M. Starnini, A. Baronchelli, and R. Pastor-Satorras, Modeling human dynamics of face-to-face interaction networks, *Phys. Rev. Lett.* **110**, 168701 (2013).
- [49] Y.-Q. Zhang, J. Cui, S.-M. Zhang, Q. Zhang, and X. Li, Modelling temporal networks of human face-to-face contacts with public activity and individual reachability, *Eur. Phys. J. B* **89**, 26 (2016).
- [50] M. Starnini, M. Frasca, and A. Baronchelli, Emergence of metapopulations and echo chambers in mobile agents, *Sci. Rep.* **6**, 31834 (2016).
- [51] M. A. R. Flores and F. Papadopoulos, Similarity forces and recurrent components in human face-to-face interaction networks, *Phys. Rev. Lett.* **121**, 258301 (2018).
- [52] V. Colizza, R. Pastor-Satorras, and A. Vespignani, Reaction–diffusion processes and metapopulation models in heterogeneous networks, *Nat. Phys.* **3**, 276 (2007).
- [53] H. W. Hethcote, An immunization model for a heterogeneous population, *Theor. Pop. Biol.* **14**, 338 (1978).
- [54] R. M. May and R. M. Anderson, Spatial heterogeneity and the design of immunization programs, *Math. Biosci.* **72**, 83 (1984).
- [55] A. L. Lloyd and R. M. May, Spatial heterogeneity in epidemic models, *J. Theor. Biol.* **179**, 1 (1996).
- [56] B. Grenfell and J. Harwood, (Meta) population dynamics of infectious diseases, *Trends Ecol. Evol.* **12**, 395 (1997).
- [57] B. T. Grenfell and B. M. Bolker, Cities and villages: Infection hierarchies in a measles metapopulation, *Ecol. Lett.* **1**, 63 (1998).
- [58] I. Hanski, Metapopulation dynamics, *Nature* **396**, 41 (1998).
- [59] I. A. Hanski, M. E. Gilpin, and D. E. McCauley, *Metapopulation Biology* (Elsevier, San Diego, 1997).
- [60] I. A. Hanski and O. E. Gaggiotti, *Ecology, Genetics and Evolution of Metapopulations* (Academic Press, Burlington, 2004).
- [61] V. Colizza and A. Vespignani, Invasion threshold in heterogeneous metapopulation networks, *Phys. Rev. Lett.* **99**, 148701 (2007).
- [62] V. Colizza and A. Vespignani, Epidemic modeling in metapopulation systems with heterogeneous coupling pattern: Theory and simulations, *J. Theor. Biol.* **251**, 450 (2008).
- [63] A. Barrat, M. Barthélemy, and A. Vespignani, *Dynamical Processes on Complex Networks* (Cambridge University Press, Cambridge, 2008).
- [64] M. Chinazzi *et al.*, The effect of travel restrictions on the spread of the 2019 novel coronavirus (COVID-19) outbreak, *Science* **368**, 395 (2020).
- [65] H. W. Lau and K. Y. Szeto, Asymptotic analysis of first passage time in complex networks, *EPL* **90**, 40005 (2010).
- [66] H. Sedrakyan and N. Sedrakyan, *Algebraic Inequalities* (Springer, Cham, 2018).
- [67] A.-L. Barabási and R. Albert, Emergence of scaling in random networks, *Science* **286**, 509 (1999).
- [68] D. J. Watts and S. H. Strogatz, Collective dynamics of ‘small-world’ networks, *Nature* **393**, 440 (1998).
- [69] N. Masuda, H. Miwa, and N. Konno, Geographical threshold graphs with small-world and scale-free properties, *Phys. Rev. E* **71**, 036108 (2005).
- [70] A. Lancichinetti, S. Fortunato, and F. Radicchi, Benchmark graphs for testing community detection algorithms, *Phys. Rev. E* **78**, 046110 (2008).
- [71] V. Batagelj and A. Mrvar, Pajek datasets, <http://vlado.fmf.uni-lj.si/pub/networks/data/> (2006).
- [72] L. Lotero, R. G. Hurtado, L. M. Floría, and J. Gómez-Gardeñes, Rich do not rise early: Spatio-temporal patterns in the mobility networks of different socio-economic classes, *R. Soc. Open Sci.* **3**, 150654 (2016).
- [73] D. Balcan and A. Vespignani, Phase transitions in contagion processes mediated by recurrent mobility patterns, *Nat. Phys.* **7**, 581 (2011).
- [74] V. Belik, T. Geisel, and D. Brockmann, Natural human mobility patterns and spatial spread of infectious diseases, *Phys. Rev. X* **1**, 011001 (2011).
- [75] C. Poletto, M. Tizzoni, and V. Colizza, Human mobility and time spent at destination: Impact on spatial epidemic spreading, *J. Theor. Biol.* **338**, 41 (2013).
- [76] J. Gómez-Gardeñes, D. Soriano-Panos, and A. Arenas, Critical regimes driven by recurrent mobility patterns of reaction–diffusion processes in networks, *Nat. Phys.* **14**, 391 (2018).
- [77] C. Granell and P. J. Mucha, Epidemic spreading in localized environments with recurrent mobility patterns, *Phys. Rev. E* **97**, 052302 (2018).
- [78] D. Soriano-Panos, G. Ghoshal, A. Arenas, and J. Gómez-Gardeñes, Impact of temporal scales and recurrent mobility patterns on the unfolding of epidemics, *J. Stat. Mech.* (2020) 024006.
- [79] I. Scholtes, N. Wider, R. Pfützner, A. Garas, C. J. Tesse, and F. Schweitzer, Causality-driven slow-down and speed-up of diffusion in non-markovian temporal networks, *Nat. Commun.* **5**, 5024 (2014).
- [80] M. Rosvall, A. V. Esquivel, A. Lancichinetti, J. D. West, and R. Lambiotte, Memory in network flows and its effects on spreading dynamics and community detection, *Nat. Commun.* **5**, 4630 (2014).
- [81] A. Feldmann and W. Whitt, Fitting mixtures of exponentials to long-tail distributions to analyze network performance models, *Perform. Evaluation* **31**, 245 (1998).
- [82] L. Gauvin, M. Génois, M. Karsai, M. Kivelä, T. Takaguchi, E. Valdano, and C. L. Vestergaard, Randomized reference models for temporal networks, Preprint arXiv:1806.04032 (2018).
- [83] N. Alon, I. Benjamini, E. Lubetzky, and S. Sodin, Non-backtracking random walks mix faster, *Commun. Contemp. Math.* **9**, 585 (2007).
- [84] R. Fitzner and R. van der Hofstad, Non-backtracking random walk, *J. Stat. Phys.* **150**, 264 (2013).